Symmetry breaking of localized discrete matter waves induced by spin-orbit coupling

M. Salerno
Dipartimento di Fisica "E.R. Caianiello", CNISM and INFN - Gruppo Collegato di Salerno, Universitá di Salerno, Via Giovanni Paolo II, 84084 Fisciano (SA), Italy

F. Kh. Abdullaev
Department of Physics, Kulliyyah of Science, International Islamic University of Malaysia, 25200 Kuantan, Pahang, Malaysia
(Dated: 16 June 2015)

We study localized nonlinear excitations of a dilute Bose-Einstein condensate (BEC) with spin-orbit coupling in a deep optical lattice (OL). For this we introduce a tight-binding model that includes the spin-orbit coupling (SOC) at the discrete level in the form of a generalized discrete nonlinear Schödinger equation. Existence and stability of discrete solitons of different symmetry types is demonstrated. Quite interestingly, we find three distinctive regions in which discrete solitons undergo spontaneously symmetry breaking, passing from on-site to inter-site and to asymmetric, simply by varying the interatomic interactions. Existence ranges of discrete solitons with inter-site symmetry depend on SOC and shrink to zero as the SOC parameter is increased. Asymmetric discrete solitons appear as novel excitations specific of the SOC. Possible experimental implementation of these results is briefly discussed.

I. INTRODUCTION

Presently there is a growing interest in the study of Bose-Einstein condensates (BEC) in the presence of non abelian gauge fields that mimic magnetic interactions. In particular, spin-orbit couplings (SOC) of Rashba and Dresselhaus types and their combinations, have been recently realized in binary BEC mixtures in the presence of trapping potentials $V(x)$ of different types [1–3]. As well known, the SOC represents a major source of intra-atomic magnetic interaction. In solid state physics it plays an important role in the magnetism of solids, well described in terms of individual ions, as it is for earth rare insulators. In general, however, in solids the SOC is a rather weak source of magnetic interaction, largely superseded by the electrostatic effects, and very difficult (if not impossible) to enhance. The situation is quite different in Bose-Einstein condensates where a variety of synthetic spin-orbit couplings can be generated and managed by mens of external laser fields. BECs with SOC, indeed, represents ideal systems to explore magnetic phenomena difficult to achieve in a solid state context, such as: new quantum phases with unusual magnetic properties, existence of stripe modes [4], fractional topological insulators [5–7], Majorana fermions, antiferromagnetic states [8] etc.

The interplay of SOC with interatomic interactions (nonlinearities) and periodicity of the OL, also leads to the existence of SOC solitons [9, 10]. Gap solitons in BEC with periodic Zeeman field were recently discussed in [11] (for a review of BEC in OL with SOC see [12]). In this context, different settings for the spatial periodicity have been considered: periodicity in each separate component [13, 14], periodicity in the Raman coupling [15], periodicity in the Zeeman field [11, 16–18]. Dispersion relations of one-dimensional BEC with SOC in OL were also experimentally investigated [19] and existence of flat bands and superfluidity in BEC with SOC was demonstrated in [13]. Array of vortex lattices in shallow optical lattices [14] and vortices in 2D optical lattices [20] have been also investigated. The extension to quasi-periodic OL and the Anderson localization of BEC with effective SOC have been considered in [21]. These studies refer mainly to the continuous case, and the effects of SOC at the discrete level (BEC arrays) appears scarcely uninvestigated.

The aim of the present letter is to consider BEC mixtures with SOC in the presence of deep optical lattices. We use Wannier functions to derive a tight-binding model that includes the SOC in the form of a generalized discrete nonlinear Schödinger equation (SO-DNLS) with typical double minima linear dispersion relations and that support modes of gap-soliton type in the presence of nonlinearity. We show that for attractive (resp. repulsive) nonlinear interactions, GS can exist in the semi-infinite gap below (resp. above) the bottom (resp. top) band, as well as in the gap between the two bands. The time evolution of attractive (resp. repulsive) fundamental GSs, e.g. with lower (resp. higher) chemical potential, are very stable while the ones located in the intra-band gap appear to be unstable at least for the parameter we considered. Quite interestingly, by increasing the strength of the intra-species interaction γ, (for simplicity assumed equal for both species) away from the linear limit, and for fixed and equal sign of the inter-species nonlinearities, we find three distinctive regions in which GS undergoes spontaneously symmetry breaking. More precisely, in the range $0 < |\gamma| < |\gamma_1|$ the GS are found to be asymmetric with respect to the lattice points, in the interval $|\gamma_1| < |\gamma| < |\gamma_2|$ they display inter-site symmetry (i.e. are symmetric with respect to the middle point between two consecutive lattice sites) and above $|\gamma_2|$ display the on-site symmetry, this behavior being observed both in the attractive and repulsive case. Asymmetric modes appear to as novel stable modes induced by the SOC.

The paper is structured as follows. In Section II the tight binding model for BEC mixtures mixtures with SOC trapped in deep optical lattice is derived. In Sec. III we derive the dispersion relation and the main properties of a BEC mixture array with SOC and all the nonlinear interactions detuned to zero. In section IV we use self-consistent exact diagonalizations of the SOC BEC mixture with SOC to investigate nonlinear spectrum (chemical potentials) and corresponding eigenfunctions (discrete solitons). In particular we investigate the occurrence of symmetry breaking as the parameters of the system are varied. Finally in Section V, the main results are summarized and possible experimental implementation settings briefly discussed.

II. TIGHT-BINDING MODEL

We consider BEC with equal contributions of Rashba and Dresselhaus SOC that can be described in the mean field approximation by the following coupled Gross-Pitaevskii equations [16**?**]:

$$\begin{aligned} i\frac{\partial \psi_j}{\partial t} &= (-\frac{\partial^2}{\partial x^2}+V(x))\psi_j - i\alpha\frac{\partial \psi_{3-j}}{\partial x}+\Omega_j\psi_j + \\ &(g_j|\psi_j|^2+g|\psi_{3-j}|^2)\psi_j, \quad j=1,2, \end{aligned} \tag{1}$$

with the linear coefficients α, $\Omega \equiv \Omega_1 = -\Omega_2$ arising from the spin orbit interaction while the nonlinear ones, g and $g_i, i = 1, 2$, are related to inter-species and intra-species scattering lengths, respectively. For the OL we take a periodic potential of the form $V(x) = V_0 cos(2x)$, the same for both components, and concentrate on the case of large amplitudes $V_0 \gg 1$ (tight binding approximation) [23]. To this regard we consider the underlying uncoupled linear periodic eigenvalue problem, e.g. with $\alpha = \Omega = 0, g = g_i = 0$, in Eq. (1),

$$\Big[-\frac{\partial^2}{\partial x^2}+V(x)\Big]\varphi_{m,k} = \varepsilon_m(k)\varphi_{m,k} \tag{2}$$

and expand the two component fields in terms of Wannier functions as

$$\psi_1 = \sum_{n,m} u_n(t)w_m(x-n),\ \psi_2 = \sum_{n,m} v_n(t)w_m(x-n). \tag{3}$$

Here $\varphi_{m,k}$ and $\varepsilon_m(k)$ denote Bloch (Floquet) functions and energy band, with m the band index and k the Bloch wavenumber taken in the first Brillouin zone, $w_m(x-n)$ are Wannier functions satisfying the orthonormal condition $\int w_j(x-n)^* w_{j'}(x-n')dx = \delta_{j,j'}\delta_{n,n'}$, and u_n , v_n are time dependent expansion coefficients to be fixed in such a manner that Eq. (1) is satisfied. Notice that in the expansions (3) appear the same Wannier functions since the underlying periodic problem is the same for both BEC components. In the following we restrict only to one band, so we drop the index m. By substituting (3) in Eq. (1) and projecting the resulting equations along the $w(x-n)$ function, one arrives at the following coupled SO-DNLS system

$$\begin{aligned} i\frac{du_n}{dt} &= -\Gamma(u_{n+1}+u_{n-1}) + i\frac{\sigma}{2}(v_{n+1}-v_{n-1}) + \Omega u_n + \\ &(\gamma_1|u_n|^2+\gamma_{12}|v_n|^2)u_n, \\ i\frac{dv_n}{dt} &= -\Gamma(v_{n+1}+v_{n-1}) + i\frac{\sigma}{2}(u_{n+1}-u_{n-1}) - \Omega v_n + \\ &(\gamma_{12}|u_n|^2+\gamma_2|v_n|^2)v_n, \end{aligned} \tag{4}$$

with

$$\begin{aligned} &\Gamma \equiv \Gamma_{n,n+1} = \int w(x-n)^*\frac{\partial^2}{\partial x^2}w(x-(n+1)dx, \\ &\gamma_i = g_i\int |w(x-n)|^4dx,\ \ \gamma_{12} = g\int |w(x-n)|^4dx, \\ &\sigma \equiv \sigma(n,n+1) = 2\alpha\int w(x-n)^*\frac{\partial}{\partial x}w(x-n-1)dx. \end{aligned} \tag{5}$$

In the derivation of Eq. (4) the following relations among coefficients have been used: $\Gamma(n,n+1) = \Gamma(n,n-1)$, $\sigma(n,n) = 0$, $\sigma(n,n-1) = -\sigma(n-1,n) = -\sigma(n,n+1)$. Moreover, due to the strong localization of the Wannier functions around the lattice sites, the sums on n have been restricted to on-site and to next neighbor sites only, for non diagonal and diagonal terms, respectively. We remark that similar models were considered also in Ref. [25].

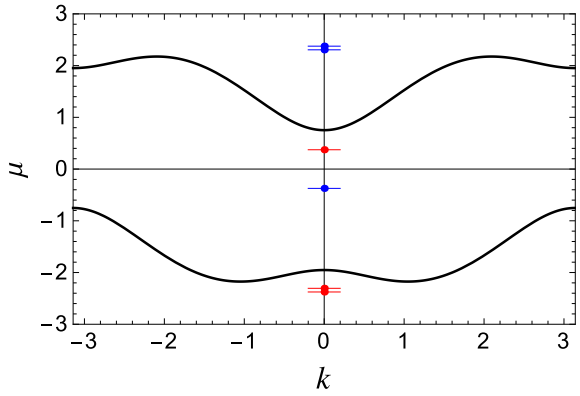

FIG. 1: Chemical potential vs k in the reciprocal space for the DNLS chain with SO coupling for the linear case $\gamma_1 = \gamma_2 = \gamma = 0$ and parameter values $\Gamma = 0.3, \Omega = 1.352, \sigma = 1.5$. The red and blue dots represent chemical potentials of localized modes for the nonlinear cases: $\gamma_1 = \gamma_2 = -0.65, \gamma_{12} = -1.8$ (attractive case), and $\gamma_1 = \gamma_2 = 0.65, \gamma_{12} = 1.8$ (repulsive case), respectively.

III. LINEAR CHAIN WITH SOC

Let us first consider the case of a linear chain with SOC ($\gamma_{12} = \gamma_i = 0,\ i = 1, 2$ in Eq. (4). From physical point of view this corresponds to a one-dimensional array of BEC in deep optical lattice in the presence of SO interaction and with all the scattering lengths detuned to zero. As usual, we consider solutions of the form $u_n = Ae^{i(kna-\omega t)}$, $v_n = Be^{i(kna-\omega t)}$ with wavenumber $k_n = 2\pi/Ln$ varying in the first Brillouin zone $[-\pi/a, \pi/a]$, with $-N/2 \leq n \leq N/2$, $L = Na$ the length of the chain, a the lattice constant fixed below without loss of generality to $a = 1$. Substituting u_n, v_n into the dynamical equations leads to a system for coefficients A, B whose compatibility conditions gives the dispersion relation:

$$\omega(k)_{\pm} = -2\Gamma\cos(k) \pm \sqrt{\Omega^2 + \sigma^2\sin^2(k)}. \tag{6}$$

It is worth to note that the upper and lower branches of the dispersion curves are related by

$$\omega_{\pm}(k) = -\omega_{\mp}(k + \pi). \tag{7}$$

Also notice the presence of two degenerated minima at $\pm k_-$ on the ground state branch and two degenerated maxima at $\pm k_+$ on the upper branch, with $k_\pm$ given by $k\pm = \pm arcos\Big[\pm\frac{2\Gamma}{\sigma}\sqrt{\frac{\sigma^2+\Omega^2}{\sigma^2+4\Gamma^2}}\Big]$. The dispersion curve in the first Brillouin zone is depicted for typical parameter values in Fig. 1. One can readily show that the amplitudes of the two component modes must be related by $(\frac{B}{A})_{\pm} = \frac{csc(k)}{\sigma}(\Omega \mp \sqrt{\Omega^2 + \sigma^2\sin^2(k)})$. Also, by combining k_+ and k_- modes one gets stationary ω_+ and ω_- stripe solutions.

IV. DISCRETE SOLITONS AND SYMMETRY BREAKING INDUCED BY SOC

In the presence of nonlinearity, localized modes with chemical potentials in the forbidden zones of the band structure (discrete gap-solitons) appear. In particular, one expects that for attractive (resp. repulsive) inter and intra-species interatomic interactions, gap-solitons to form with chemical potentials just below local minima (maxima) of the dispersion relation. This is indeed what one finds from a numerical self-consistent diagonalization of the stationary eigenvalue problem associated to Eq. (1) (see discrete levels in Fig. 1). In Fig. 2a are shown existence curves of gap-solitons of the DNLS with SO coupling for the case $\gamma_{12} < 0$ and for equally attractive intra-species interactions $\gamma_1 = \gamma_2 \equiv \gamma < 0$. The lower two branches correspond to the ground localized modes in the lower semi-infinite gap while the top curve refers to a mode inside the interband gap. In remaining panels of Fig. 2 are shown the imaginary and real parts of the component profiles u_n (blue lines) and v_n (red lines) of the gap solitons for the different values of γ corresponding to black, blue and red points depicted in panel a. It is worth to note that there is a phase difference of $e^{i\pi/2}$ between the u_n and v_n components (v_n being real and u_n purely imaginary) as well as different symmetry properties with respect to the lattice sites for the two components. Also notice that the symmetry properties of the modes change as the intra-species interactions are varied. In general, the following situation is observed. For a fixed

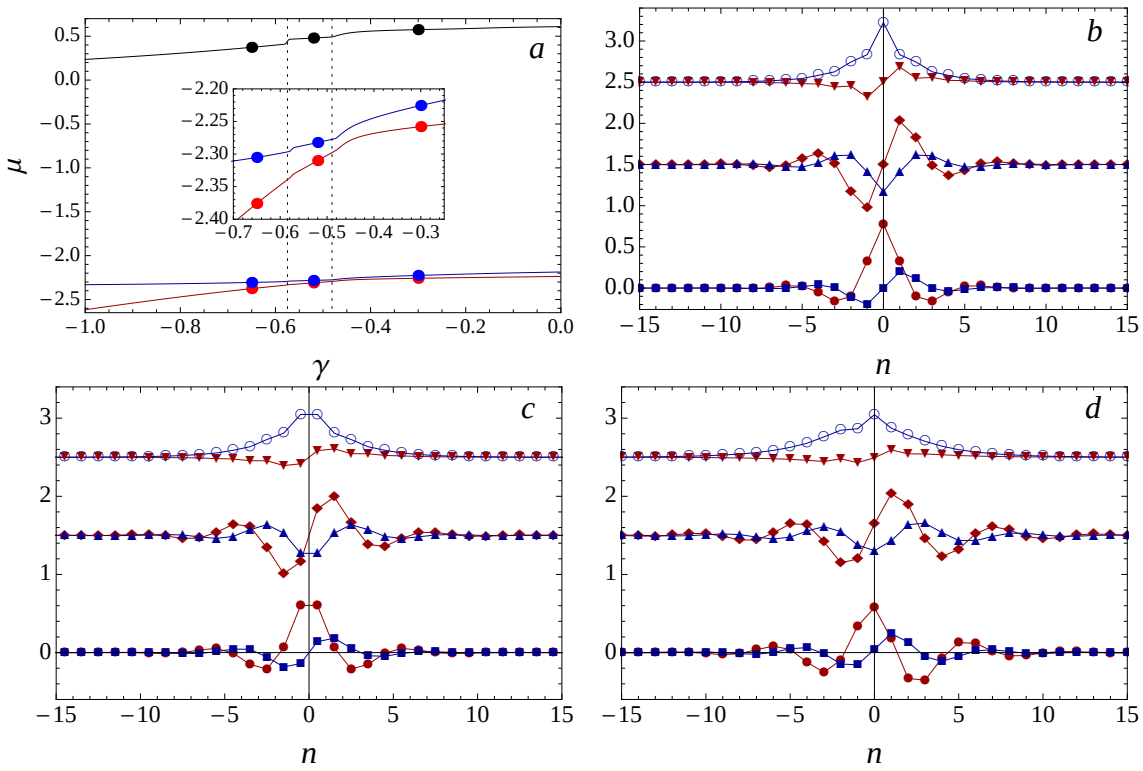

FIG. 2: Panel a). Existence curves of the localized modes of the DNLS with SO coupling as a function of the equally attractive intra-species interaction $\gamma \equiv \gamma_1 = \gamma_2$ for parameters $\Gamma = 0.3, \Omega = 1.352, \sigma = 1.5$ and fixed intra-species interaction $\gamma_{12} = -1.8$. The inset display details of the bottom curves, enlarged along the vertical axis. Panels (b), c and (d) show u_n (blue lines) and v_n (red lines) profiles of gap solitons at $\gamma = -0.65$ (panel (b)), $\gamma = -0.52$ (panel (c)) and $\gamma = -0.3$ (panel (d)), corresponding to red points (bottom profiles), blue points (middle profiles) and black points (top profiles) shown in panel (a) (in all cases v_n is purely real while u_n is purely imaginary). Middle and top profiles in all panels are shifted upward by 1.5 and 2.5, respectively, to avoid overlappings. Vertical dotted lines separate regions of different symmetry type.

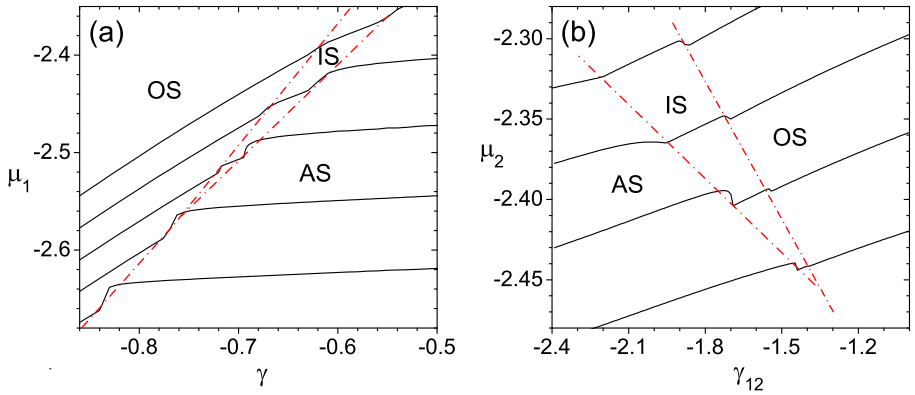

FIG. 3: Panel (a). Existence curves of ground state modes of Eq. (4) as a function of $\gamma \equiv \gamma_1 = \gamma_2$, for $\gamma_{12} = -1.8$ and different values of $\sigma = 1.6, 1.7, 1.8, 1.9, 2.0$, corresponding to black curves from top to bottom, respectively. Panel (b). Same as in panel (a) but for first excited modes of Eq. (4) as a function of γ_{12}, for different values of the intra-species interactions $\gamma_1 = -0.4$, $\gamma_2 = -0.6$ and different values of $\sigma = 1.5, 1.6, 1.7, 1.8$ (top to bottom curves, respectively). Other parameters are fixed as in Fig. 2. In both panels red dot-dashed lines separate existence regions for asymmetric (AS), inter-site symmetric (IS) and on-site symmetric (OS) modes.

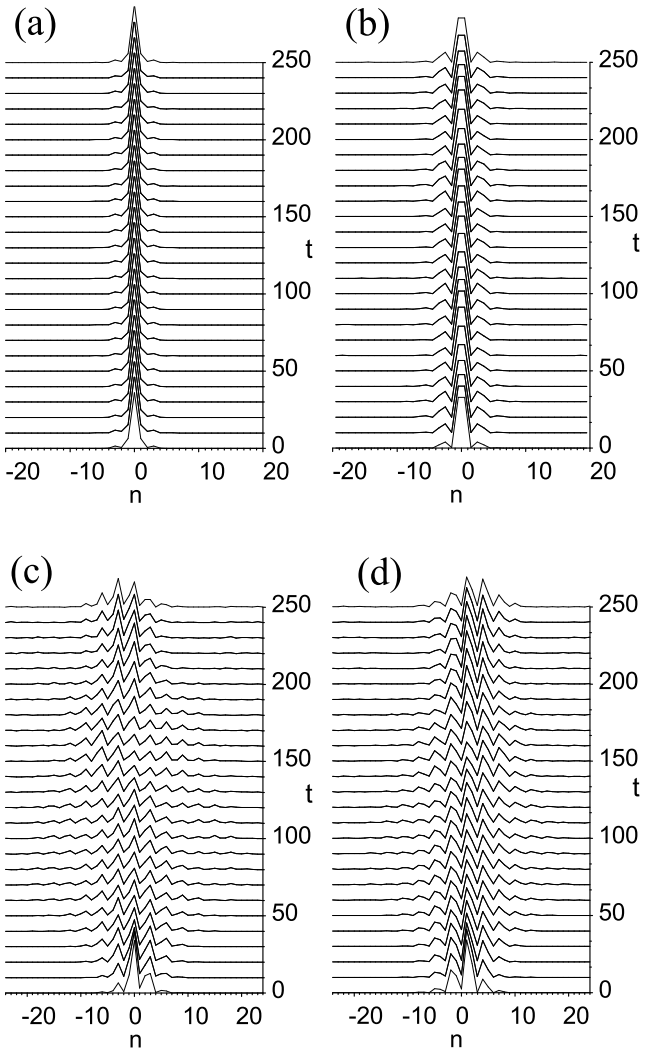

FIG. 4: Panels a-b. Time evolution of the ground state modes in Fig. 2b (panel a) and Fig. 2c (panel b) at $\gamma = -0.65$ and $\gamma = -0.52$, respectively. Panels c-d. Time evolution of the ground state (panel c) and first excited state (panel d) in Fig. 2d for the case $\gamma = -0.3$. For graphical convenience we depicted in the panels the modulo square of the v_n component only. Other parameters are fixed as in Fig. 2.

attractive inter-species nonlinearity, we find three distinctive regions in which GS undergoes spontaneously symmetry breaking as the strength of the attractive intra-species interactions (assumed equal e.g. $\gamma_i \equiv \gamma$, for simplicity) away from the $\gamma = 0$ limit. More precisely, in the range $-0.35 < \gamma < 0$ the GS are found to be asymmetric (AS) with respect to the lattice points, in the interval $-0.6 < \gamma < -0.35$ they display inter-site symmetry (IS) with respect to the middle point between two consecutive lattice sites and for $\gamma < -0.6$ they display on-site symmetry (OS). Notice that the borders of these regions correspond to the appearance of small kinks in the existence curves depicted in Fig. 2a. Also notice that the kinks at the left border of the middle region separating the modes with on-site symmetry (see panel (b)) from the ones with intra-site symmetry (see panel (c)), both of symmetric or anti-symmetric type, are sharper than the ones on the right border where modes becoming asymmetric (see panel (c)). This is further investigated in Fig.3 where the different symmetry regions for ground state and first excited state are shown for different values of σ and different nonlinearities. From panel (a) it is clear that by increasing the SOC parameter σ the IS-symmetry

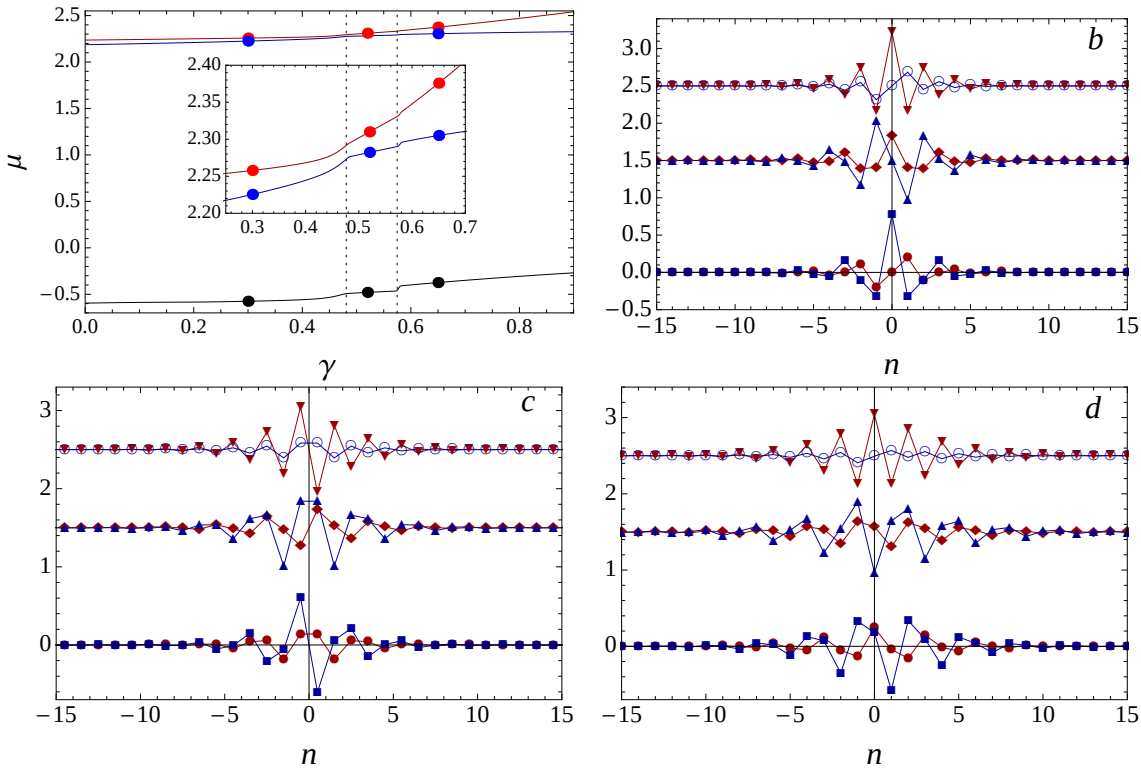

FIG. 5: Top left panel. Existence curves of the localized modes of the DNLS with SO coupling as a function of the equally repulsive intraspecies interaction $\gamma \equiv \gamma_1 = \gamma_2$ for parameters $\gamma = 0.3, \Omega = 1.352, \sigma = 1.5$ and fixed intraspecies interaction $\gamma_{12} = 1.8$. The inset display details of the top curves, enlarged along the vertical axis. Panels (b), (c) and (d) show u_n (blue lines) and v_n (red lines) profiles at $\gamma = 0.65$ (panel (b)), $\gamma = 0.52$ (panel (c)) and $\gamma = 0.3$ (panel (d)), corresponding to black points (bottom profiles), blue points (middle profiles) and red points (top profiles) in panel (a), respectively (in all cases v_n is purely real while u_n is purely imaginary). Middle and top profiles in the b,c,d, panels are shifted upward by 1.5 and 2.5, respectively, to avoid overlapping. Vertical dotted lines separate regions of different symmetry type.

region gradually shrinks to a point beyond which on a single line exists separating on-site symmetric ground states from asymmetric ones. The same phenomenon is observed for more generic choices of parameters such as the ones considered in panel (b) where γ_{12} is taken as varying parameter with γ_1, γ_2 fixed to different values (same is true also for the ground state). Notice that in this last case asymmetric modes emerge at large values of $|\gamma_{12}|$, while for the transitions driven by the intra-species parameter $|\gamma|$ in Fig.3(a), it is just the opposite. We also remark that the fact that IS solitons can become non degenerated ground states with energy lower than the one of the OS mode is just due to the interplay between SOC and nonlinearity. To the best of our knowledge, this phenomena does not exist in ordinary (e.g. without SOC) discrete or continuous coupled GPE.

Dynamical properties of the nonlinear modes have been investigated by direct numerical integrations of the DNLS-SO with small noise component added to the initial condition to check stability. Typical examples are depicted in Figs. 3-4. In general we find that on-site symmetric modes are very stable while inter-site symmetric modes stability is achieved in general only for the ground state. Asymmetric modes of the region $\gamma < -0.3$ also appear to be stable (or long lived) under time evolution, as one can see form Fig. 4. The existence of last modes appears to be specific of the SO coupling. Stability properties of localized modes in the gap appear to be critical. In particular, for the parameter range we have explored, none was found to be stable independently from symmetry type.

Similar results are also found for the case of all repulsive interactions. By reversing signs of all the interactions the chemical potentials of the discrete solitons change their signs (see Fig. 1), meaning that what was said before for lowest modes applies now to highest modes. Shape and symmetries of these modes, however, are different for the two cases, as one can see by comparing Fig. 5 with Fig. 2. Also notice the symmetry of corresponding existence curves with appearance of kinks at the critical points. Existence ranges and Dynamical properties of highest excited states are also quite similar to the ones discussed for lowest lying states states of the previous case, with the intraband gap

solitons typically unstable (not shown for brevity).

V. CONCLUSIONS

In conclusion we considered a tight-binding model for BEC with SOC and showed that stable nonlinear modes can change their symmetry from on-site symmetric to inter-site symmetric and to fully asymmetric as the nonlinearity is varied. Also, we found that the region for existence of modes with the IS symmetry shrinks to zero as the SOC parameter σ is increased. Asymmetric modes appear to be intrinsic of the SOC. Before closing this paper we remark that possible experimental implementations of the above results could be made by referring to a setting similar to the one considered in [16, 22]. For ^{87}Rb the SOC considered in this work could be realized using the tripod scheme with three laser beams [16] or the scheme used for creating tunable Rashba and Dresselhaus SOC [22]. The deep optical lattice can be generated with two additional beams with $\lambda_L = 1540$nm [19] and potential strength $V_0/E_R > 10$, where $E_R = \hbar^2 k^2/2m$ being the recoil energy [23, 24]. For the case of all attractive interactions, stable nonlinear modes in semi-infinite gap should exist for wide range of number of atoms. The symmetry transitions of the modes should then be observed by changing the scattering lengths by means of the Feshbach resonance technique.

Acknowledgements M. S. acknowledges partial support from the Ministero dell'Istruzione, dell'Universitá e della Ricerca (MIUR) through a PRIN (Programmi di Ricerca Scientifica di Rilevante Interesse Nazionale) 2010-2011 initiative, grant n.o $2010HXAW77-005$.

[1] Y.-J. Lin, K. Jimenez-Garcia, and I. B. Spielman, Nature (London) **471**, 83 (2011).
[2] V. Galitski and I. B. Spielman, Nature **494**, 49 (2013).
[3] J. Dalibard, F. Gerbier, G. Juzeliunas, and P. Ohberg, Rev. Mod. Phys. **83**, 1523 (2011).
[4] T.-L. Ho and S. Zhang, Phys. Rev. Lett. **107**, 150403 (2011).
[5] Y. Li, L. P. Pitaevskii, and S. Stringari, Phys. Rev. Lett. **108**, 225301 (2012).
[6] M. Levin, and A. Stern, Phys. Rev. Lett. **103**, 196803 (2009).
[7] T.A. Sedrakyan, ,A. Kamenev, and L. I. Glazman, Phys. Rev. A **86**, 063639 (2012).
[8] D.A. Zezyulin, R. Driben, V.V. Konotop, B.A. Malomed, Phys. Rev. A **88**, 013607 (2013).
[9] V. Achilleos, D. J. Frantzeskakis, P. G. Kevrekidis, and D. E. Pelinovsky, Phys. Rev. Lett. **110**, 264101 (2013).
[10] L. Salasnich and B. A. Malomed Phys. Rev. A **87**, 063625 (2013).
[11] Y. Kartashov, V.V. Konotop, and F. Kh. Abdullaev, Phys.Rev.Lett. (2013).
[12] S. Zhang, W. S. Cole, A. Paramekanti, and N. Trivedi, arXive:1411.2297.
[13] Y. Zhang and C. Zhang, Phys. Rev. A **87**, 023611 (2013).
[14] H Sakaguchi and B. Li, Phys. Rev. A **87**, 015602 (2013).
[15] V. Ya. Demikhovski , D. V. Khomitsky, and A. A. Perov, Low Temp. Phys. **33**, 115 (2007).
[16] M. J. Edmonds, J. Otterbach, R. G. Unanyan, M. Fleischhauer, M. Titov, and P. Ohberg, New J. Phys. **14**, 073056 (2012).
[17] K. Jimenez-Garcia, L. J. LeBlanc, R. A. Williams, M. C. Beeler, A. R. Perry, and I. B. Spielman, Phys. Rev. Lett. **108**, 225303 (2012).
[18] Y. Zhang, Li Mao, and C. Zhang, Phys. Rev. Lett. **108**, 035302 (2012).
[19] C. Hamner, Y. Zhang, M. A. Khamehchi, M. J. Davis, and P. Engels, arXiv:1405.4048v1.
[20] V. E. Lobanov, Y. V. Kartashov, and V.V. Konotop, Phys.Rev.Lett. **112**, 180403 (2014).
[21] L. Zhou, H. Pu and W. Zhang, Phys. Rev. **A 87**, 023625 (2013).
[22] D.L. Campbell, G. Juzeliunas, and I.B. Spielman, Phys.Rev. A **84**, 025602 (2011).
[23] G. L. Alfimov, P. G. Kevrekidis, V. V. Konotop, and M. Salerno, Phys. Rev. E **66**, 046608 (2002).
[24] O. Morsch and M. Oberthaler, Rev. Mod. Phys. **78**, 179 (2006).
[25] P.P. Belicev, G. Gligoric, J. Petrovic, A. Maluckov, L. Hadievski, B.A.Malomed, J.Phys. B 48 (2015) 065301.